Adv Compos Hybrid Mater (2018) 1:114–126
DOI 10.1007/s42114-017-0011-4

REVIEW

Metal oxides for thermoelectric power generation and beyond

Yining Feng[1] · Xiaodong Jiang[1] · Ehsan Ghafari[1] · Bahadir Kucukgok[1,2] · Chaoyi Zhang[1] · Ian Ferguson[3] · Na Lu[1,2,4]

Received: 11 April 2017 / Revised: 10 May 2017 / Accepted: 20 May 2017 / Published online: 2 November 2017

Abstract Metal oxides are widely used in many applications such as thermoelectric, solar cells, sensors, transistors, and optoelectronic devices due to their outstanding mechanical, chemical, electrical, and optical properties. For instance, their high Seebeck coefficient, high thermal stability, and earth abundancy make them suitable for thermoelectric power generation, particularly at a high-temperature regime. In this article, we review the recent advances of developing high electrical properties of metal oxides and their applications in thermoelectric, solar cells, sensors, and other optoelectronic devices. The materials examined include both narrow-band-gap (e.g., Na_xCoO_2, $Ca_3Co_4O_9$, BiCuSeO, $CaMnO_3$, $SrTiO_3$) and wide-band-gap materials (e.g., ZnO-based, SnO_2-based, In_2O_3-based). Unlike previous review articles, the focus of this study is on identifying an effective doping mechanism of different metal oxides to reach a high power factor. Effective dopants and doping strategies to achieve high carrier concentration and high electrical conductivities are highlighted in this review to enable the advanced applications of metal oxides in thermoelectric power generation and beyond.

✉ Na Lu
luna@purdue.edu

[1] Lyles School of Civil Engineering, Sustainable Materials and Renewable Technology (SMART) Laboratory, Purdue University, West Lafayette, IN, USA

[2] Birck Nanotechnology Center, Purdue University, West Lafayette, IN, USA

[3] College of Engineering and Computing, Missouri University of Science and Technology, Rolla, MO, USA

[4] School of Materials Engineering, Purdue University, West Lafayette, IN, USA

Keywords Oxides · Thermoelectric · Power factor · Solar cells · Optoelectronic power generation

1 Introduction

Thermoelectric (TE) materials have the ability to directly convert heat into electricity for power generation via the Seebeck effect [1, 2]. It can play a crucial role in renewable energy production since 60% of energy produced worldwide is waste as the form of heat. Additionally, as a solid-state device, TE technology has many attractive features such as high reliability, environmental friendliness, and no moving parts [3].

Despite recent advances in TE research, the potential impact of TE technology for power generations is hindered by the heavy usage of toxic, rare, and expensive (e.g., Te and Se) elements and their low power output. For instance, there are only three major TE material systems commercially available for from low- to high-temperature regimes including Bi_2Te_3 (300–500 K) [4], PbTe (500–600 K) [5], and SiGe (600–800 K) [6]. Their applications, particularly Te-based materials, are largely restricted by the toxicity, limited element resources, and material degradation at high temperatures [7, 8].

Metal oxides, on the other hand, are promising candidates to circumvent these challenges due to their earth abundancy, low cost, non-toxicity, and high thermal stability [9–11]. More importantly, their electronic properties can be tuned from insulator behavior to metallic behavior by manipulating their crystal structures, chemical compositions, and doping concentrations [12, 13]. These unique material properties open an exciting opportunity to obtain high power output in metal oxides. In fact, for TE power generation applications, a material with high power factor is even more important than having a high efficiency, since most waste heat sources are free (e.g., waste heat from car exhaust, gas engine) and unlimited (e.g.,

solar radiations) [14]. To this end, the focus of this review article is on examining the metal oxide potentials for TE power generation with an emphasis on materials with high power factor. Effective doping strategies in achieving high power factor are highlighted for various metal oxides, particularly, Na_xCoO_2 [15], $Ca_3Co_4O_9$ [16], BiCuSeO [17], $CaMnO_3$ [18], $SrTiO_3$ [19], ZnO-based [20], SnO_2-based [21], and In_2O_3-based [22] alloys. More broadly, recent advancement of metal oxides for potential commercial applications in thermal- and electrical-related fields is summarized, which includes TE power generators, solar cells, and sensors.

2 Fundamental physics of thermoelectric metal oxides

The quality of materials for TE application is described by a dimensionless parameter ZT [7], which is defined as the following:

$$\mathrm{ZT} = \frac{S^2\sigma}{\kappa} T \tag{1}$$

where S is the Seebeck coefficient, σ is the electrical conductivity, and k is the thermal conductivity. In physics, k consists of the electronic part (k_e, due to carrier transport) and lattice part (k_{Ph}, due to phonon transport). The term $S^2\sigma$ is called the power factor (PF). A high PF indicates that a TE power generator can achieve a high power output.

Seebeck coefficient (S, in V/K) is an intrinsic material property, which measures the thermoelectric voltage induced in response to a temperature difference across the material. S represents the energy difference between the averaged charge carrier energy versus the Fermi energy. It can be expressed as the following:

$$S = \left(\frac{k_B}{-q}\right)\left(\frac{E_c - E_F}{k_B T} + \frac{\Delta_n}{k_B T}\right) \tag{2}$$

where E_F is the Fermi level, in which the dependence on the temperature (T) and the Boltzmann constant (k_B) is made explicit. For semiconductors, the Seebeck value can be negative (electron conduction) or positive value (hole conduction); therefore, the absolute value is more important. For doped semiconductors, the relationship between the Seebeck coefficient and carrier concentration can be expressed as the following:

$$S = \frac{8\pi^2 {k_B}^2}{3eh^2} m^* T \left(\frac{\pi}{3n}\right)^{2/3} \tag{3}$$

where k_B is the Boltzmann constant, e is the carrier charge, h is Planck's constant, m^* is the effective mass of the charger carrier, and n is the carrier concentration. As can be seen, lower carrier concentration is desirable for materials to reach high Seebeck coefficient.

Electrical conductivity (σ) describes the ease of conducting charge carrier transport of a material, which is defined as:

$$\sigma = ne\mu \tag{4}$$

where n is the carrier concentration, e is the carrier charge, and μ is the mobility. To reach high electrical conductivity, a high carrier concentration is desirable; however, it often degenerates the Seebeck coefficient of materials as governed by Eq. (3). Therefore, an optimized carrier concentration of TE materials is often found at 10^{19}–10^{21}/cm^3 [23]. The electrical conductivity of ideal TE materials is usually on the order of 10^3 (S/cm); however, the electrical conductivity of metal oxides is often lower, on the order of 10–10^2 (S/cm). Thus, the investigation of effective doping mechanism on improving electrical conductivity without degenerating the Seebeck coefficient is crucial to enable their applications in TE power generation and related fields.

Thermal conductivity (k), on the other hand, is the parameter that describes how efficiently a material can conduct heat. In the case of semiconductors, the total thermal conductivity (κ_T) consists of contributions from both electron and phonon transports, defined as the following:

$$\kappa_T = \kappa_e + \kappa_l \tag{5}$$

where κ_e and κ_l are, respectively, the electron and lattice thermal conductivities. κ_l is known as the most important mechanism for heat conduction in semiconductors at temperatures close to room temperature, which normally accounts for 90% contributions in wide-band-gap materials.

For good TE materials, the typical value of thermal conductivity is $k_T < 2$ W/mK [24]. Low thermal conductivity can be seen intuitively as an important parameter to maintain a certain temperature gradient across the junctions, which is essential for reaching high ZT in a material system [25]. Otherwise, the temperature gradient would quickly turn into equilibrium and cancel the materials TE effect. Therefore, recent efforts in TE materials research have been heavily focused on reducing thermal conductivity to achieve high ZT using various strategies, such as nano-structuring, phonon rattling, and band structuring as reported in previous studies [26–28]. To this end, most previous review articles focus on examining various mechanisms to achieve low thermal conductivity of materials. Very few literatures have discussed mechanisms to reach high power output of TE materials [29], and none of them focused on metal oxides.

Unlike previous literatures, we have systematically examined effective strategies to achieve high power output for potential applications in TE power generation. Much attention is paid to examining the effective dopants of various metal oxides to achieve high electrical conductivity without degrading

the Seebeck value or vice versa. As such, this review article will pave the road to the development of cost-effective, earth-abundant, and high-performance metal oxides for TE power generation and other thermal-electrical-related applications.

3 TE properties of metal oxides

3.1 Narrow band gap

3.1.1 Na_xCoO_2

Na_xCoO_2 is composed of the alternating stacks of sodium-ion (Na^+) plane and CoO_2 plane along with the *c*-axis, with a hexagonal layered crystal structure. Phonon and electron transports follow different paths in this structure. The electrons/holes are transported by passing through the CdI_2-type CoO_2 layer for *p*-type electronic conduction, while the disordered charge-balancing Na^+ layer is providing the path for phonons. The materials with this kind of layered structure are so-called "phonon glass electronic crystals," which often show high electrical conductivity with low thermal conductivity [30], an ideal material property for thermoelectric applications. Therefore, the *p*-type alkali cobalt oxide-based compounds have been recognized as the most promising oxide TE materials [16, 31, 32]. Additionally, the polycrystalline $Na_{0.85}CoO_2$ was reported to exhibit PF as high as 14×10^{-4} W/mK^2 at 300 K [15, 33]. The quite high PF values of either single or polycrystalline Na_xCoO_2 indicate its great potential for TE power generation.

The TE properties of polycrystalline Na_xCoO_2 have been widely investigated with different dopants and doping level of Na_xCoO_2. The effects of different metal dopants on the PF values of Na_xCoO_2 are shown in Fig. 1. It was found that

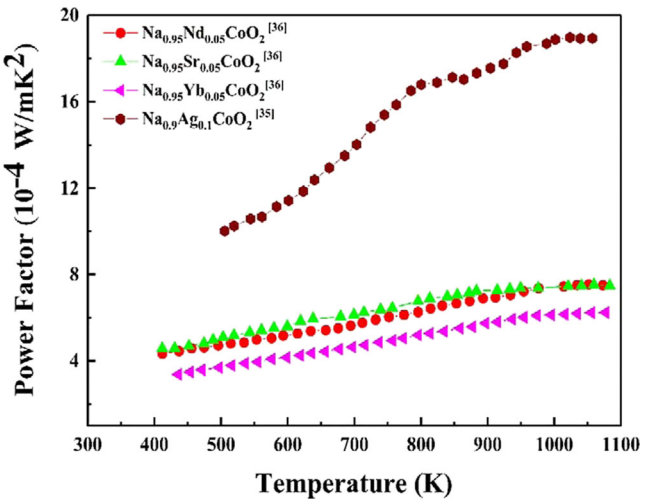

Fig. 1 Power factor values of Na_xCoO_2 with different dopants as a function of temperature

silver (Ag) doping is the most effective because it can improve the electrical conductivity and the Seebeck coefficient of Na_xCoO_2 simultaneously, resulting in an enhanced PF value. Ag, as a metal-phase dopant, can obviously increase the electrical conductivity, but the mechanism of Ag doping enhancing the Seebeck value is still unclear. It could be caused by the uniform Ag doping in the samples or the electron-electron correlation [34]. With 10% Ag doping, Na_xCoO_2 achieved the PF as high as 18.92×10^{-4} W/mK^2 at ~ 1100 K with the carrier density of ~ 10^{21}/cm^3 [35]. Compared with un-doped $NaCoO_2$, other dopants (Y, Nd, Sr, Sm) have little effects on improving PF values [36], and some dopants (Ni, Yb) even have negative effects [36, 37]. Because of the interdependent relations between the Seebeck coefficient and electrical conductivity, these dopants often improve one while they degrade the other. In contrast, doping transition metal elements turn out to be more effective in improving the PF of Na_xCoO_2 composites.

3.1.2 $Ca_3Co_4O_9$

$Ca_3Co_4O_9$ is another promising *p*-type TE material due to its high Seebeck coefficient and electrical conductivity [38–40]. The crystal structure of $Ca_3Co_4O_9$ is similar to Na_xCoO_2, which is stacked by the CdI_2-type CoO_2 layer and Ca_2CoO_3 layer (rock salt-type structure) alternatively along the *c*-axis. For $Ca_3Co_4O_9$, the CoO_2 planes of $Ca_3Co_4O_9$ are mainly responsible for electrical conduction while the interlayers (Ca_2CoO_3) between the CoO_2 planes transfer the heat by phonons. The un-doped polycrystalline $Ca_3Co_4O_9$ shows the Seebeck coefficient, electrical conductivity, and PF of 150 μV/K, 80 S/cm, and 1.5×10^{-4} W/mK^2, respectively, at room temperature [41]. It was reported that doping noble metals, such as Ag, at the Ca cationic atom site can simultaneously increase the Seebeck coefficient and electrical transport properties, thus resulting in an enhanced PF [42]. This is mainly due to the substitution of Ag^+ for Ca^{2+} in $Ca_{3-x}Ag_xCo_4O_9$ ($0 < x < 0.3$) which results in more improvement for the Fermi-level E_F than that for the valence band energy E_V of the crystal system [43]. For thermoelectric materials, the Seebeck coefficient is proportional to $E_F - E_V$. Therefore, it can be concluded that Ag doping in $Ca_3Co_4O_9$ enhances the Seebeck coefficient. Although the PF value of Na_xCoO_2 is much larger than that of $Ca_3Co_4O_9$ at 300 K, $Ca_3Co_4O_9$ is being more widely used in TE applications because of its high stability on compositional changes [44].

The doping effects of different transition metal (TM) elements on the PF of $Ca_3Co_4O_9$ are shown in Fig. 2. With the temperature increasing from 300 to 1000 K, the PF of the polycrystalline $Ca_3Co_4O_9$ with different dopants increased [29, 45–47]. It can be found that the substitution of transition elements (Fe, Bi, Mn, Ba, Ga) for Ca or Co has a positive effect on the PF improvement of $Ca_3Co_4O_9$. Fe is the most

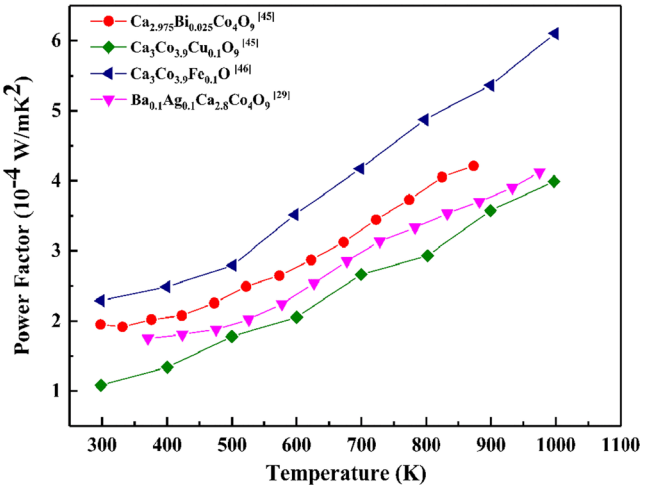

Fig. 2 Power factor values of $Ca_3Co_4O_9$ doped with the transition metal elements as a function of temperature

effective dopant which has drastically increased the PF of $Ca_3Co_4O_9$ from 2.3 × 10^{-4} to 6.10 × 10^{-4} W/mK^2 at ~ 1000 K. Fe ions replace the Co ions in the CoO_2 layers, and this substitution changes the electronic structure and increases the electronic correlations. Thus, doping Fe causes an enhancement in both the Seebeck coefficient and electrical conductivity [46]. On the other hand, doping Cu and Ag decreases the PF value because Cu/Ag ions mainly occupy the sites of Co ions in the Ca_2CoO_3 layers, which results in an increase of electrical conductivity but a decrease of the Seebeck coefficient.

3.1.3 BiCuSeO

BiCuSeO oxyselenide was first reported as a promising TE material in 2010 [48]. BiCuBeO belongs to the layered ZrCuSiAs-type structure with the tetragonal space group *P4/nmm* [49]. The crystal structure is alternately stacked by $(Bi_2O_2)^{2+}$ layers and $(Cu_2Se_2)^{2-}$ layers along with the *c*-axis. The $(Bi_2O_2)^{2+}$ layers are mainly responsible for the carrier (holes) transport while the $(Cu_2Se_2)^{2-}$ layers are for reserving charges. The un-doped polycrystalline BiCuSeO shows the Seebeck coefficient and electrical conductivity of 350 μV/K and 1.12 S/cm at 300 K, respectively, leading to a low PF of 0.14 × 10^{-4} W/mK^2 [49]. This is mainly due to the low electrical conductivity caused by the intrinsic low carrier concentration of 1 × 10^{18}/cm^3. This value is much lower than the optimized doping concentration of TE materials (10^{19}–10^{21}/cm^3) [50–53]. To enhance the TE properties of BiCuSeO, the alkaline-earth metals (Mg, Ca, Ba, and Sr) with 2^+ valence have been reported to be good *p*-type dopants replacing the Bi^{3+} in BiCuSeO [49, 54–56]. Doping these elements can improve the electrical conductivity by increasing the carrier concentration, which leads to an enhancement of PF.

Figure 3 summarizes the different metal dopants on the PF values of $Bi_{1-x}M_xCuSeO$ (M = Mg, Ca, Sr and Ba). As shown, the PF of BiCuSeO was greatly improved by doping M^{2+} compared to its undoped crystal structure. The electrical transport properties of BiCuSeO change from semiconducting behavior to metallic behavior once M^{2+} is doped, resulting in a significant increase in electrical conductivity without degrading the Seebeck coefficient. Among all the dopants, Ba^{2+} doping resulted in the highest electrical conductivity in the $Bi_{0.875}Ba_{0.125}CuSeO$ sample, which reached 535 S/cm at 300 K [55]. Thus, the largest PF (~ 6.14 × 10^{-4} W/mK [2]) was achieved at 900 K. With the Ba^{2+} modulation doping, the PF of BiCuSeO has achieved PF as high as 10 × 10^{-4} W/mK^2 at ~ 900 K [17], which is the highest PF value of doped BiCuSeO ever reported.

Alkali metals, such as Na, have also shown promises in improving the PF of BiCuSeO [57], but the limitation of solubility in BiCuSeO impeded their potential as good *p*-type dopants. Recently, Pb/Ca co-doping has been reported as an efficient way to enhance the TE properties of BiCuSeO [17, 58]. Under Pb/Ca co-doping, the PF of BiCuSeO has reached ~ 10 × 10^{-4} W/mK^2 at room temperature [58].

3.1.4 $CaMnO_3$

Perovskite oxide $CaMnO_3$ has been considered as a good *n*-type TE material due to its high Seebeck coefficient in the range of − 300 μV/K~− 400 μV/K [59–62] and chemical stability at temperatures up to 1200 K [63]. Although $CaMnO_3$ has relatively high Seebeck coefficient, its electrical conductivity is very low (0.1 to 1 S/cm in the temperature range 300–1000 K), which often results in low PF values [64]. Previous studies indicated that with a minor electron

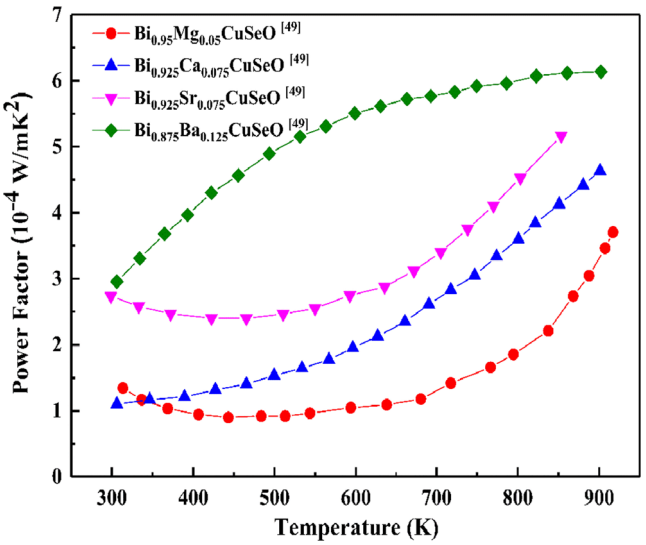

Fig. 3 Power factor values of $Bi_{1-x}M_xCuSeO$ (M = K, Mg, Ca, Sr, and Ba) as a function of temperature

doping at the A (Ca^{2+}) and B sites (Mn^{4+}), its electrical conductivity can be significantly increased. As such, the high PF of $CaMnO_3$ TE materials has been achieved by replacing the A site and B site with rare-earth ions, Y^{3+}, Bi^{3+}, and Nb^{5+} and Ta^{5+}, Mo^{6+}, and W^{5+}, respectively [65].

Ohtaki et al. reported that the electron transport properties of $CaMnO_3$ have been improved by replacing the A site and B site with different lanthanides [18, 60, 66] and heterovalent cations such as W, Ta, Ru, Mo, and Nb [67–71], respectively. Several studies have been carried out to investigate the TE properties of $CaMnO_3$, particularly focusing on strategies to increase the electrical conductivity without significantly decreasing the Seebeck coefficient. Figure 4 exhibits the PF of single and co-doped $CaMnO_3$ with respect to temperature. Clearly, Bi-substituted $CaMnO_3$ shows the largest PF of all the samples. Doping larger cations such as Bi^{3+} on the Ca site results in high electrical conductivity caused by the higher mobility of the carriers [60]. The highest PFs of 4.67×10^{-4} W/mK^2 at 423 K and 3.74×10^{-4} W/mK^2 at 965 K were achieved for $Ca_{1-x}Bi_xMnO_3$ with a Bi composition at $x = 0.03$ (Fig. 4) [72]. However, the co-doped $Ca_{0.96}Bi_{0.04}Mn_{0.96}Nb_{0.04}O_3$ sample shows a lower PF because of the decrease of the electrical conductivity. Compared to Bi-substituted $CaMnO_3$, the increased amount of Nb^{5+} into the MnO_6 octahedra leads to a more serious lattice distortion [73]. As a result, the electrical conductivity is decreased due to a reduction in carrier mobility, which leads to the lower PF of the co-doped $Ca_{0.96}Bi_{0.04}Mn_{0.96}Nb_{0.04}O_3$ sample.

Lan et al. [74] studied the TE properties of polycrystalline $Ca_{1-x}Gd_xMnO_3$ ($x = 0.02$, 0.04, and 0.06) synthesized via a chemical co-precipitation method. The maximum electrical conductivity of 113.4 S/cm was discovered for Gd-doped $CaMnO_3$ sample at $x = 0.06$, which resulted in the highest PF of 2.3×10^{-4} W/mK^2 at 950 K, shown in Fig. 4. Nag et al. [75] examined the transport properties of the co-substituted $Ca_{1-x}Gd_xMn_{1-x}Nb_xO_3$ ($0 \le x \le 0.1$) perovskite synthesized by solid-state reaction. The increase of electrical conductivity can be attributed to the formation of Mn^{3+}, which results in the increase of carrier concentration. However, the Seebeck coefficient is lower in co-doped $CaMnO_3$ samples due to the high carrier concentration, which results in a relatively low PF of 2.0×10^{-4} W/mK^2 at 800 K.

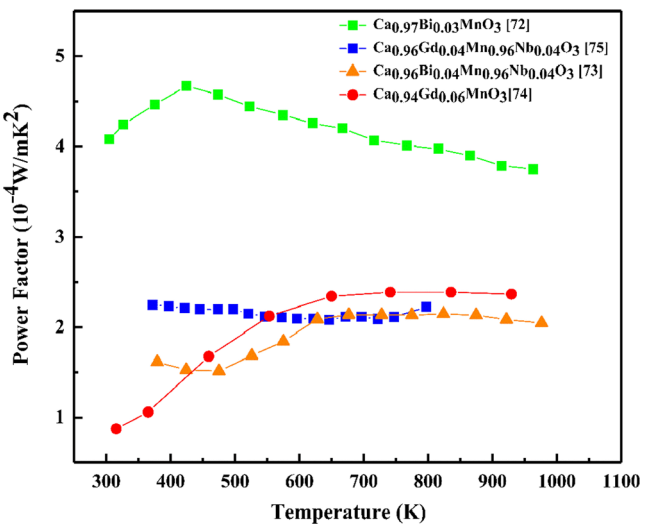

Fig. 4 Power factor values of doped $CaMnO_3$ with various dopants as a function of temperature

3.1.5 $SrTiO_3$

Strontium titanate ($SrTiO_3$)-based perovskite oxide materials have shown *n*-type electrical conduction behavior, and they have an ideal cubic crystal structure (space group *pm3m*, lattice parameter $a = 0.3905$ nm at 300 K, and melting point 2353 K) [63, 76]. Recently, $SrTiO_3$ has been recognized as a promising candidate for low-temperature TE applications, since it has good electrical conductivity and large Seebeck coefficient (~ 100 μV/K) at high doping concentration ($n \sim 10^{21}$ cm^{-3}) [30]. This is mainly due to its high electron mobility (10 to 100 cm^2/V/s) [30] and large effective mass ($m^* \sim 2$–16 m_0) [77–79], which arises from its *d*-band nature and conduction band degeneracy [80, 81]. Furthermore, the electrical conductivity of the $SrTiO_3$ can be changed from insulating to metallic behaviors through different doping mechanisms such as introducing oxygen vacancies or substitutional doping of the Sr^{2+} or Ti^{4+} sites with higher-valence elements (e.g., La^{3+} for Sr^{2+} sites or Nb^{5+} for Ti^{4+} sites) [79, 82, 83].

Okuda et al. [81] first reported the highest PF 28–36 $\times 10^{-4}$ W/mK^2 at 300 K for heavily La-doped $SrTiO_3$ single crystals with doping concentration of 0.2–2 $\times 10^{21}$/cm^3, which is comparable to that of Bi_2Te_3, the state-of-the-art low-temperature TE material. The unexpectedly high PF is due to the large Seebeck coefficient (~ 350 μV/K) caused by the high degeneracy of the conduction band as well as the large energy-dependent scattering rate. Also, heavily Nb-doped $SrTiO_3$ single crystals at carrier concentration of 3.3×10^{21}/cm^3 achieved high PF (~ 20×10^{-4} W/mK^2) at 300 K. The high Seebeck coefficient (~ 240 μV/K) at room temperature was caused by the large effective mass ($m^* \sim 7.3$–7.7 m_0) [80].

Figure 5 shows that $Sr_{0.95}La_{0.05}TiO_3$ reaches the highest PF of 28×10^{-4} W/mK^2 at 320 K due to the large Seebeck coefficient as discussed before. Since Sm, Dy, and Y are rare-earth elements, they have smaller ionic radius compared to Sr^{2+}, which results in a decreased lattice parameter [84]. Compared to La-doped $SrTiO_3$, the La- and Dy-co-doped $La_{0.08}Dy_{0.12}Sr_{0.8}TiO_3$ sample has lower PF due to the decreased electrical conductivity. The electrical conductivity

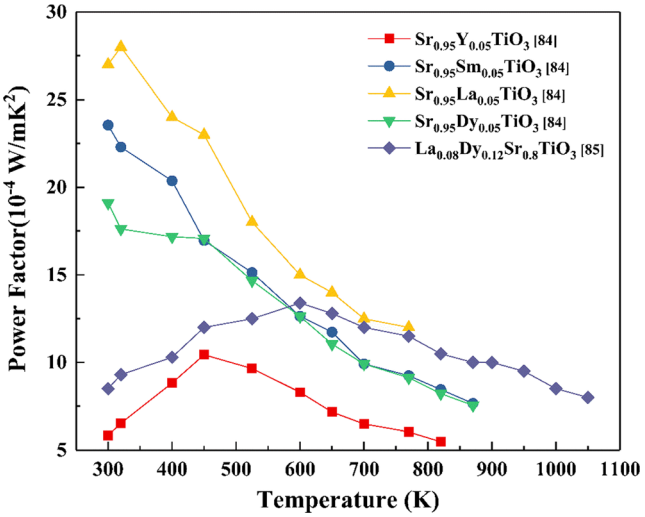

Fig. 5 Power factor values of doped $SrTiO_3$ with various dopants as a function of temperature

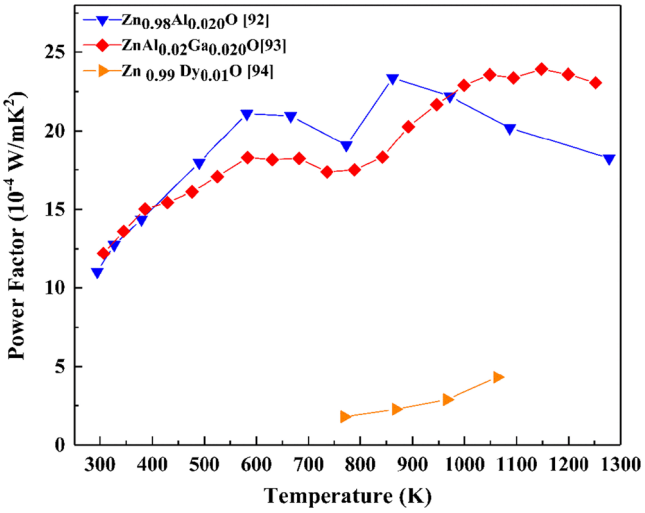

Fig. 6 Power factor values of doped ZnO with various dopants as a function of temperature

decreases can be attributed to the reduced carrier mobility caused by the formation of the second phase ($Dy_2Ti_2O_7$) during the doping mechanism [85]. However, Y-doped $SrTiO_3$ has the lowest PF mainly due to the low Seebeck coefficient.

3.2 Wide band gap

3.2.1 ZnO-based

Zinc oxide (ZnO) has a direct wide band gap of 3.37 eV and large exciton-binding energy of 60 meV [86, 87]. It is a non-toxic, low-cost, and earth-abundant material which is stable at a high temperature. These properties make it a promising candidate for *n*-type TE materials for energy harvesting in high-temperature applications [88–90]. At room temperature, Lu et al. has reported that the PF of bulk ZnO materials was achieved at about 0.75×10^{-4} W/mK^2 at carrier concentration ($n \sim 10^{-17}$/cm^3), due to the high crystal quality resulting in a large Seebeck coefficient (~ 478 μV/K) [91].

Figure 6 presents the temperature-dependent PF of ZnO-based TE materials. A general trend of PF increasing with the increase of temperature can be observed, and Al has been used as the most common dopant to enhance the TE properties of ZnO. Despite the high Seebeck for the Al-doped nano-bulk and bulk ZnO samples, the electrical conductivity of these samples is extremely low leading to a small PF value. Compared to their nano-structured counterparts, the bulk $Zn_{0.96}Al_{0.02}Ga_{0.02}O$ and $Zn_{0.98}Al_{0.02}O$ alloys showed a higher PF in the temperature range from 300 to ~ 1300 K [92, 93], which can be attributed to a better crystal quality in the bulk materials leading to higher electrical conductivity. Because the doped Al^{3+} and Ga^{3+} usually substitute for Zn^{2+} in ZnO and act as *n*-type donors, these dopants significantly enhance the electrical property of ZnO. Furthermore, the largest PF value (23.9×10^{-4} W/mK^2) was obtained in bulk $Zn_{0.96}Al_{0.02}Ga_{0.02}O$ at ~ 1147 K reported by Ohtaki et al. [93], which remains the highest PF of all high-temperature *n*-type oxides that was ever reported.

The addition of a small amount of Dy_2O_3 has been also found to be effective for improving the thermoelectric properties of ZnO [94]. The highest power factor of 4.46×10^{-4} W/mK^2 at 1100 K was obtained for $Zn_{0.995}Dy_{0.005}O$. The PF is approximately 56 times larger than that of undoped ZnO (0.08×10^{-4} W/mK^2 at 1100 K) [94]. It was reported that the addition of Dy_2O_3 leads to an increase in the electrical conductivity, which can be attributed to the substitution of Dy^{3+} for Zn^{2+}. As a result, this increased carrier concentration of the system can compensate for the electrical charge balance [94].

3.2.2 SnO_2-based

Tin oxide (SnO_2) is a wide-band-gap (3.6 eV) semiconductor that crystallizes in a rutile-type structure [95]. Due to its electrical and optical properties, SnO_2 and impurity-doped SnO_2 are mainly used as an electrode for dye-sensitized solar cell [95] and electrochromic devices [96], a catalyst in chemical reactions [97], a varistor [98], and a gas sensor [99].

Rubenis et al. [100] reported that the TE properties of $Sn_{1-x}Sb_xO_2$ (x = 0, 0.01, 0.03, 0.05) were synthesized by spark plasma sintering and subsequently air annealing at 1173 K. The addition of Sb_2O_5 increased the carrier concentration of SnO_2. Thus, the Seebeck coefficient decreased but the electrical conductivity increased up to a maximum of 5.5 times at the Sb-doping level of x = 0.03. The $Sn_{0.99}Sb_{0.01}O_2$ sample has the highest PF value of 4.5×10^{-4} W/mK^2 at 1073 K.

Figure 7 shows that $Sn_{0.94}Sb_{0.03}Zn_{0.03}O_2$ reaches the maximum PF of 2.13×10^{-4} W/mK^2 at 1060 K, which is 126% higher

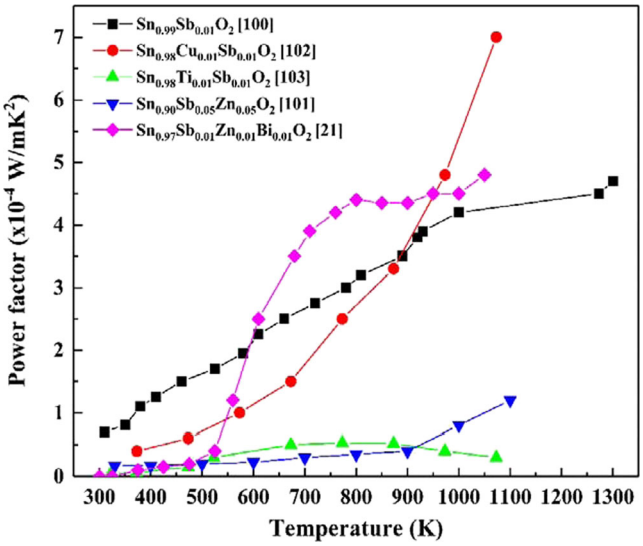

Fig. 7 Power factor values of doped SnO_2 with various dopants as a function of temperature

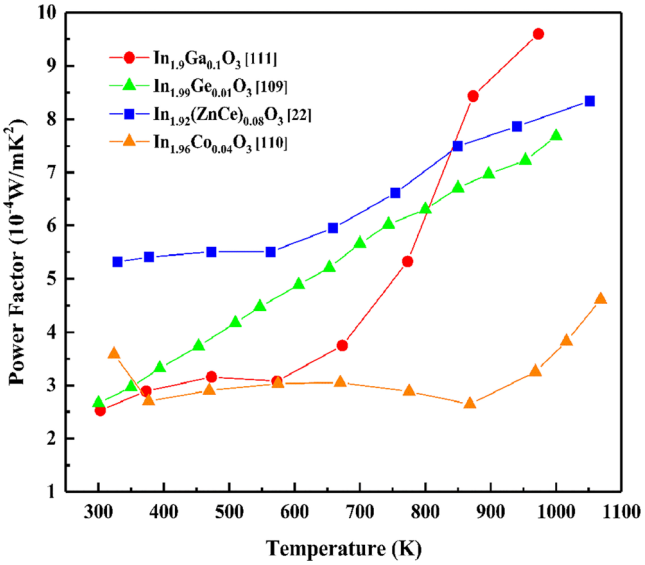

Fig. 8 Power factor values of doped In_2O_3 with various dopants as a function of temperature

than that of the undoped sample. The electrical conductivity increases are due to the carrier concentration that was caused by an increase in Sb doping and the density of Zn doping [101]. Moreover, the Bi-doped $Sn_{0.97}Sb_{0.01}Zn_{0.01}Bi_{0.01}O_2$ sample has reached the maximum PF of 4.8×10^{-4} W/mK^2 at 1060 K. Yanagiya et al. [21] reported that Bi increased the electrical conductivity by increasing the number of free electrons in SnO_2, where Bi behaves as a donor. Also, the addition of CuO to the Sb-doped SnO_2 increased the PF at a high temperature ($T > 1000$ K). The substitution of Cu for Sn decreased carrier concentration because Cu is divalent but Sn is quadrivalent. As a result, the Seebeck coefficient increased. Also, the addition of the CuO has significantly improved the relative density of SnO_2 ceramics [102]. As such, the electrical conductivity increased with the increased carrier mobility. The Cu- and Sb-co-doped $Sn_{0.98}Cu_{0.01}Sb_{0.01}O_2$ reached the highest PF value of 7×10^{-4} W/mK^2 at 1073 K. However, Ti- and Sb-co-doped $Sn_{1-x-y}Ti_ySb_xO_2$ samples had lower PF values due to the electrical conductivity decreases with adding more TiO_2 because TiO_2 dissolved in SnO_2 that caused the reduction of the mobility, resulting in the decrease of the electrical conductivity [103].

3.2.3 In_2O_3-based

Indium oxide (In_2O_3) is a semiconductor with a band gap of 3.6 eV, [104] which has recently gained interest as a promising candidate for high-temperature TE applications due to its high stability at air. It has been shown that the electrical properties of In_2O_3 can be drastically changed by doping with Sn, Mo [105, 106], Zr, Ti [107, 108], and W [109].

Figure 8 shows that $In_{1.92}(ZnCe)_{0.08}O_3$-nanostructured ceramic exhibits the highest PF of 8.36×10^{-4} W/mK^2 at 1050 K[22]. This is due to the influence of nanostructuring and point defects on TE properties of the In_2O_3 system. Point defect hinders the atomic-scale scattering and improves the carrier concentration thereby increasing PF. Utilizing the spark plasma-sintering process, co-doped polycrystalline In_2O_3 ceramics were fabricated by Liu et al. [110]. They have achieved high electrical conductivity and Seebeck coefficient, which resulted in PF of 4.53×10^{-4} W/mK^2 at 1070 K for $In_{1.96}Co_{0.04}O_3$. Later, Liu et al. [111] prepared single-element Ga-doped In_2O_3 ceramics by spark plasma sintering to explore their TE properties at high temperatures. The slight change in the Seebeck coefficient and a significant enhancement of the electrical conductivity (~ 400 S/cm) at 973 K were caused by an increase of carrier concentration through doping Ga, which achieved the highest PF of 9.6×10^{-4} W/mK^2 in $In_{1.90}Ga_{0.10}O_3$ at 973 K.

Table 1 summarizes the TE properties of various metal oxides with different dopants at a high-temperature regime, approximately 800 K. It has shown that metal oxides have good TE performance at high-temperature range. For *n*-type materials, the highest PF value was found as of 22×10^{-4} W/mK^2 for $Zn_{0.98}Al_{0.02}O$, which is close to that of SiGe, the state-of-the-art high-temperature TE material. For *p*-type materials, the highest PF value was reported as 16×10^{-4} W/mK^2 for $Na_{0.95}Ag_{0.05}CoO_2$, which is lower than that of *n*-type materials. Despite *p*-type materials having high Seebeck coefficient caused by the large effective mass of the hole, their electrical conductivity is much lower due to the difficulty of doping. Thus, the investigation of effective doping mechanisms is very important, particularly for *p*-type TE materials, to explore more applications such as solar cells, transistors, sensors, and photodetectors.

Table 1 Thermoelectric properties of metal oxides measured at 800 K by different dopants, S is for Seebeck Coefficient, σ is for electrical conductivity, and PF is for power factor

Material	Dopants	$\|S\|$ (μV/K)	σ (S/cm)	k (W/mK)	PF ($\times 10^{-4}$ W/mK^2)	Ref.
Narrow band gap, *p*-type						
Na_xCoO_2	Y	149.5	271.9	1.72	6.08	[36]
	Nd	150.0	280.8	1.43	6.32	[36]
	Sr	156.2	276	1.37	6.73	[36]
	Sm	145.4	271.8	1.38	5.75	[36]
	K	140.0	313	1.35	6.13	[36]
	Yb	139.0	268	1.47	5.18	[36]
	Ag	205.2	392.1	1.34	16.51	[35]
$Ca_4Co_4O_2$	Bi	166.7	145.76	–	4.05	[45]
	Fe	234.7	88.41	1.92	4.87	[46]
	Ga	173.6	114.17	1.52	3.44	[47]
BiCuSeO	Mg	352.2	30	0.33	3.72	[49]
	Sr	202.4	110.30	0.30	4.52	[49]
	Ba	170.0	207	0.25	5.98	[49]
Narrow band gap, *n*-type						
$CaMnO_3$	Gd	147	113	1.41	2.44	[74]
	Bi	206	95.87	1.62	4.07	[72]
	Bi, Nb	166	77.6	1.82	2.14	[73]
	Gd, Nb	150	100	1.2	2.25	[75]
$SrTiO_3$	La	210	250	5.5	11.03	[84]
	Sm	223	126	–	6.27	[84]
	Gd	206	130	–	5.52	[84]
	Dy	200	140	–	5.60	[84]
	La, Dy	159	420	3.46	10.62	[85]
Wide band gap, *n*-type						
ZnO	Al	163	839	12	22.29	[92]
	Al, Ga	173	611	6.2	18.29	[93]
	Dy	55	80	–	0.24	[94]
SnO_2	Sb	150	190	11.5	4.28	[100]
	Cu, Sb	70	100	7	0.49	[102]
	Ti, Sb	65	100	2.1	0.42	[103]
	Sb, Zn	150	15	–	0.34	[101]
	Sb, Zn, Bi	125	290	–	4.53	[21]
In_2O_3	Ga	150	375	0.25	8.44	[111]
	Co	203	65	–	2.68	[110]
	Zn, Ge	126	428	3.2	6.79	[22]

S Seebeck coefficient, *σ* electrical conductivity, *PF* power factor

In summary, transitional metal elements are effective dopants for metal oxides to reach high power factor. For Na_xCoO_2, Ag has proven to be a good dopant as it increases both electrical conductivity and Seebeck coefficient simultaneously, which results in the highest PF value for *p*-type metal oxides. For *n*-type oxides, both $CaMnO_3$ and $SrTiO_3$ have shown good TE performance, particularly with Bi and La doping, respectively. For wide-band-gap materials, Ga-doped In_2O_3 has shown promising TE properties for high-TE-power-generation applications.

4 Commercial application of metal oxides for TE power generation and beyond

4.1 TE device for power generation

As a heat engine, the efficiency of thermoelectric device is governed by the Carnot efficiency and the materials' figure of merit ZT as the following:

$$\eta = \frac{T_H - T_C}{T_H}\left(\frac{\sqrt{1+ZT}-1}{\sqrt{1+ZT}+T_C/T_H}\right) \quad (6)$$

where T_H, T_C, and T_M are the hot-side, cold-side, and average temperatures, respectively. As a cost-effective alternative to conventional TE materials, oxides have superior thermal stability to be used for devices operated at a high-temperature regime to achieve higher Carnot efficiency (theoretical maximum) $\eta_C = (T_H - T_C)/T_H$, thus achieving much higher energy efficiency for power generation.

The simplest design of TEG consists of a *p*-leg and *n*-leg connected by conducting strips in series and covered by ceramic plate with heat conduction in perpendicular. Matsubara et al. [112] reported that a fin-type-oxide thermoelectric device was fabricated by using $Ca_{2.75}Gd_{0.25}Co_4O_9$ as *p*-leg and $Ca_{0.92}La_{0.08}MnO_3$ as *n*-leg. The high power density of the TE device was achieved at 21 mW/cm^2 at $\Delta T = 390$ K. This high performance was observed in oxide-based thermoelectric generators, because the power factor of both *p*- and *n*-type materials increased with temperature, with no bipolar effect observed. Another oxide-based TE device was fabricated from Man's group using $CaMgO_2$(CMO-25-42S) as TE module [113]. A large power density of 92 mW/cm^2 was reported at $\Delta T = 440$ K compared to the previous study. It is interesting to note that the power outputs, in both cases, are sufficient to power small electronics, sensors, and other optoelectronic devices. Intriguingly, metal oxide-based TE generators have shown great promises for high-temperature power generation through waste heat harvesting.

4.2 Solar cells

In solar cell application, metal oxides such as SnO_2 [95], ZnO [114], and $SrTiO_3$ [115] are often used as photoelectrodes in dye solar cells (DSCs) [116, 117]. DSCs are made by a layer of dye-anchored mesoporous metal oxides, known as photoelectrodes, and covered with conducting glass plates on both sides [118]. Like TEG devices, efficiency is also important for solar cells. The efficiency of DSC is defined as [119]

$$\eta = \frac{J_{SC} V_{OC} FF}{P_{IN}} \tag{7}$$

where J_{SC} is current per unit active area, V_{OC} is open-circuit voltage, FF is fill factor, and P_{IN} is power input.

Durrant et al. have fabricated a DSC with ZrO_2-doped TiO_2-blocking layer, which resulted in a 35% efficiency improvement and reached $V_{OC} = 50$ mV [120]. This significant efficiency improvement was attributed to the increased electron density of The ZrO_2-doped TiO_2 thin films. As such, a significant recombination loss was prevented at short-circuit condition. However, the overall efficiency of photoelectric conversion at the device level has only reached 8.1%. Comparing with the 24.7% efficiency from a silicon-based solar cell, the DSC with metal oxide photoelectrode still needs much improvement [119]. For instance, much effort is needed in synthesizing high-crystallinity metal oxides to increase charge collection efficiency in DSC without adversely affecting dye loading and, consequently, the short circuit current density.

4.3 Gas sensor application

Another related application for metal oxides is gas sensors. Gas sensors are used to detect toxic gas-like carbon monoxide (CO) and nitrous oxide (N_2O). Metal oxides are usually both thermally and chemically stable and, hence, very suitable for gas-sensing application. For example, SnO_2 and TiO_2 can be used for CO sensors, and ZnO can be used in N_2O sensors. According to Barbi [121], SnO_2-based CO sensor has the best performance at a temperature of 523 K and response (R_0/R) of 2.2 at 20 ppm. This significant improvement was attributed to the ultra-fine crystal size (400 Å) of SnO_2, which increased the free-carrier density of nanocrystals and localized the higher concentration of adatoms.

5 Summary

In this paper, we discuss recent advances in oxide-based thermoelectric materials and devices for power generation through waste heat harvesting. Metal oxides offer very promising solutions to the development of non-toxic and cost-effective thermoelectric devices for power generations. For low-temperature operation (300 K), the highest PF was found as 28.3×10^{-4} W/mK^2 in *n*-type $Sr_{0.95}La_{0.05}TiO_3$, which is in competition to that of BiTe, the state-of-the-art TE material at low-temperature regime. For high temperature (1147 K), the highest PF (23.9×10^{-4} W/mK^2) was obtained in $Zn_{0.96}Al_{0.02}Ga_{0.02}O$, which makes ZnO as the best reported *n*-type TE material.

Despite the recent advancement, metal oxides for TE power generation are still in their early stage of development, and many scientific and technological challenges need to be addressed. For instance, it is very difficult to reach high electrical conductivity of metal oxides without degrading their Seebeck value simultaneously. Achieving high doping concentration and *p*-type behavior in wide-band-gap metal oxides remains a significant challenge. Regardless, the scientific and technological importance of developing metal oxide TE materials is evident, and the outlook is very promising. Clearly, discovering effective doping mechanisms to achieve high power output is essential to the development of thermoelectric power generation, solar cells, gas sensors, and photodetectors.

Funding information The authors at Purdue University are grateful for the financial supports from National Science Foundation CAREER program (under Grants of CMMI – 1560834) and NSF IIP- 1700628, and Ross Fellowship from Purdue University.

References

1. Tritt TM (2011) Thermoelectric phenomena, materials, and applications. Annu Rev Mater Res 41:433–448
2. Shakouri A (2011) Recent developments in semiconductor thermoelectric physics and materials. Annu Rev Mater Res 41:399–431
3. Webb JH (1962) Thermoelectricity: science and engineering. J Am Chem Soc 84:690–691
4. Dresselhaus M et al (2007) New directions for low-dimensional thermoelectric materials. Adv Mater 19:1043–1053
5. Takagiwa Y, Pei Y, Pomrehn G, Snyder G (2012) Dopants effect on the band structure of PbTe thermoelectric material. Appl Phys Lett 101:092102
6. Rowe D, Shukla V (1981) The effect of phonon-grain boundary scattering on the lattice thermal conductivity and thermoelectric conversion efficiency of heavily doped fine-grained, hot pressed silicon gemanium alloy. J Appl Phys 52:7421
7. Minnich A, Dresselhaus M, Ren Z, Chen G (2009) Bulk nanostructured thermoelectric materials: current research and future prospects. Energy Environ Sci 2:466–479
8. Liu W, YaN X, Chen G, Ren Z (2012) Recent advances in thermoelectric nanocomposites. Nano Energy 1:42–56
9. Zhao HB, Hao Q, Xu DC, Lu N (2016) High-throughout ZT predictions of nanoporous bulk materials as next-genertion thermoelectric materials: a material genome approach. Phys Rev B 93:205206
10. Wei H et al (2017) Significantly enhanced energy density of magnetite/polypyrrole nanocomposite capacitors at high rates by low magnetic fields. Adv Compos Hybrid Mater. https://doi.org/10.1007/s42114-017-0003-4
11. Yang X, Jiang X, Huang Y, Guo Z, Shao L (2017) Building nanoporous metal-organic frameworks "armor" on fibers for high-performance composite materials. ACS Appl Mater Interfaces 9:5590–5599
12. Hurwitz E et al (2010) Thermopower study of gan-based materials for next-generation thermoelectric devices and applications. J Electron Mater 40:513–517
13. Lu N, Ferguson IT (2013) III-Nitrides for energy production: phtovoltaic and thermoelectric applications. Semicond Sci Technol 28:074023
14. Liu Z, Yi X, Wang J, Kang J, Melton A.G, Shi Y, Lu N, Wang J, Li J, Ferguson IT (2012) Ferromagnetism and its stability in n-type Gd-doped GaN: First-principles calculation. Appl Phys Lett 100(23):232408
15. Lee M et al (2006) Large enhancement of the thermopower in NaxCoO2 at high Na doping. Nat Mater 5:537–540
16. Ohta H, Sugiura K, Koumoto K (2008) Recent progress in oxide thermoelectric materials: p-type Ca3Co4O9 and n-type SrTiO3−. Inorg Chem 47:8429–8436
17. Pei Y-L, Wu H, Wu D, Zheng F, He J (2014) High thermoelectric performance realized in a BiCuSeO system by improving carrier mobility through 3D modulation doping. J Am Chem Soc 136:13902–13908
18. Funahashi R et al (2008) Thermoelectric properties of CaMnO3 system. Int Conf Thermoelect 124–128
19. Koumoto K, Wang YF, Zhang RZ, Kosuga A, Funahashi R (2010) Oxide thermoelectric materials: a nanostructuring approach. Annu Rev Mater Res 40:363–394. https://doi.org/10.1146/annurev-matsci-070909-104521
20. Kucukgok B, Hussain B, Zhou CL, Ferguson IT, Lu N (2015) Thermoelectric properties of zno thin film grown by metal-organic chemical vapor deposition. MRS Online Proceedings Library. Cambridge University Press, Cambridge, pp 1805
21. Yanagiya S, Nong N, Sonne M, Pryds N (2012) Thermoelectric properties of SnO2-based ceramics doped with Nd, Hf and Bi. AIP Conference Proceedings 1449:327
22. Lan JL, Lin YH, Liu Y, Xu SL, Nan CW (2012) High thermoelectric performance of nanostructured In2O3-based ceramics. J Am Ceram Soc 95:2465–2469
23. Vaqueiro P, Powell AV (2010) Rencent developments in nanostructured materials for high-performance thermoelectrics. J Mater Chem 20:9577–9584
24. Tritt TM, Subramanian MA (2006) Thermoelectric materials, phenomena, and applications: a bird's eye view. MRS Bull 31:11
25. Nolas GS, Kaeser M, Littleton RT, Tritt TM (2000) High figure of merit in partially filled ytterbium skutterudite materials. Appl Phys Lett 77:1855–1857
26. Koumoto Kunihito WY, Ruizhi Z, Atsuko K, Ryoji F (2010) Oxide thermoelectric materials: a nanostructuring approach. Annu Rev Mater Res 40:32
27. Pei Y et al (2011) Convergence of electronic bands for high performance bulk thermoelectrics. Nature 473:66–69
28. Hicks LD, Dresselhaus M (1993) Thermoelectric figure of merit of a one-dimensional conductor. Phys Rev B 47:16631. https://doi.org/10.1103/PhysRevB.47.16631
29. Zhang F, Lu Q, Zhang J (2009) Synthesis and high temperature thermoelectric properties of BaxAgyCa3−x−yCo4O9 compounds. J Alloys Compd 484:550–554
30. Nag A, Shubha V (2014) Oxide thermoelectric materials: a structure-property relationship. J Electron Mater 43:962–977. https://doi.org/10.1007/s11664-014-3024-6
31. Doumerc J-P et al (2009) Transition-metal oxides for thermoelectric generation. J Electron Mater 38:1078–1082
32. Li Q, Lin Z, Zhou J (2009) Thermoelectric materials with potential high power factors for electricity generation. J Electron Mater 38:1268–1272
33. Tong XC (2011) Chapter 11: Thermoelectric Cooling Through Thermoelectric Materials In: Advanced Materials for Thermal Management of Electronic Packaging. Springer Series in Advanced Microelectronics, vol 30. Springer, New York, NY
34. Li N et al (2009) Self-ignition route to Ag-doped Na 1.7 Co 2 O 4 and its thermoelectric properties. J Alloys Compd 467:444–449
35. Ito M, Furumoto D (2008) Microstructure and thermoelectric properties of NaxCo2O4/Ag composite synthesized by the polymerized complex method. J Alloys Compd 450:517–520
36. Nagira T, Ito M, Katsuyama S, Majima K, Nagai H (2003) Thermoelectric properties of (Na1−yMy)xCo2O4 (M= K, Sr, Y, Nd, Sm and Yb; y= 0.01~0.35). J Alloys Compd 348:263–269
37. Wang L, Wang M, Zhao D (2009) Thermoelectric properties of c-axis oriented Ni-substituted NaCoO 2 thermoelectric oxide by the citric acid complex method. J Alloys Compd 471:519–523
38. Bhaskar A, Jhang C-S, Liu C-J (2013) Thermoelectric oroperties of Ca3−xDyxCo4O9+δ with x= 0.00, 0.02, 0.05, and 0.10. J Electron Mater 42:2582–2586
39. Bhaskar A, Lin Z-R, Liu C-J (2013) Thermoelectric properties of Ca2.95Bi0.05Co4−xFexO 9+δ (0⩽ x⩽ 0.15). Energy Convers Manag 76:63–67
40. Bhaskar A, Lin Z-R, Liu C-J (2014) Low-temperature thermoelectric and magnetic properties of Ca3−xBixCo4O9+δ (0≤ x≤ 0.30). J Mater Sci 49:1359–1367
41. Tian R et al (2013) Ga substitution and oxygen diffusion Kinetics in Ca3Co4O9+δ-based thermoelectric oxides. J Phys Chem C 117:13382–13387
42. Bhaskar A, Yang Z-R, Liu C-J (2015) High temperature thermoelectric properties of co-doped Ca 3−xAgxCo3.95Fe0.05O9+δ (0≤ x≤ 0.3). Ceram Int 41:10456–10460
43. Wang Y, Sui Y, Cheng J, Wang X, Su W (2007) The thermal-transport properties of the Ca3−xAgxCo4O9 system (0≤ x≤ 0.3). J Phys Condens Matter 19:356216
44. Fergus JW (2012) Oxide materials for high temperature thermoelectric energy conversion. J Eur Ceram Soc 32:525–540

45. Cho J-Y et al (2015) Effect of trivalent bi doping on the seebeck coefficient and electrical resistivity of Ca^ sub 3^ Co^ sub 4^ O^ sub 9. J Electron Mater 44:3621
46. Wang Y, Sui Y, Wang X, Su W, Liu X (2010) Enhanced high temperature thermoelectric characteristics of transition metals doped Ca3Co4O9+δ by cold high-pressure fabrication. J Appl Phys 107:033708
47. Nong N, Liu C-J, Ohtaki M (2010) Improvement on the high temperature thermoelectric performance of Ga-doped misfit-layered Ca3Co4−xGaxO9+δ (x= 0, 0.05, 0.1, and 0.2). J Alloys Compd 491:53–56
48. Zhao L et al (2010) Bi1−xSrxCuSeO oxyselenides as promising thermoelectric materials. Appl Phys Lett 97:092118
49. Zhao L-D et al (2014) BiCuSeO oxyselenides: new promising thermoelectric materials. Energy Environ Sci 7:2900–2924
50. Sootsman JR, Chung DY, Kanatzidis MG (2009) New and old concepts in thermoelectric materials. Angew Chem Int Ed 48:8616–8639
51. Li J-F, Liu W-S, Zhao L-D, Zhou M (2010) High-performance nanostructured thermoelectric materials. NPG Asia Materials 2: 152–158
52. Kanatzidis MG (2009) Nanostructured thermoelectrics: the new paradigm? Chem Mater 22:648–659
53. Snyder GJ, Toberer ES (2008) *Complex* thermoelectric materials. Nat Mater 7:105–114
54. Li J et al (2013) Thermoelectric properties of Mg doped p-type BiCuSeO oxyselenides. J Alloys Compd 551:649–653
55. Li J et al (2012) A high thermoelectric figure of merit ZT> 1 in Ba heavily doped BiCuSeO oxyselenides. Energy Environ Sci 5: 8543–8547
56. Pei Y-L et al (2013) High thermoelectric performance of oxyselenides: intrinsically low thermal conductivity of Ca-doped BiCuSeO. NPG Asia Materials 5:e47
57. Li J et al (2014) The roles of Na doping in BiCuSeO oxyselenides as a thermoelectric material. J Mater Chem A 2:4903–4906
58. Liu Y et al (2016) Synergistically optimizing electrical and thermal transport properties of BiCuSeO via a dual-doping approach. Adv Energy Mater 6:1502423
59. Raveau B, Martin C, Maignan A (1998) What about the role of B elements in the CMR properties of ABO(3) perovskites? J Alloys Compd 275:461–467
60. Ohtaki M, Koga H, Tokunaga T, Eguchi K, Arai H (1995) Electrical-transport properties and high-temperature thermoelectric performance of (Ca(0.9)M(0.1))Mno3 (M=Y,La,Ce,Sm,in,Sn, Sb,Pb,Bi). J Solid State Chem 120:105–111
61. Flahaut D et al (2006) Thermoelectrical properties of A-site substituted Ca1-xRexMnO3 system. J Appl Phys 100:084911
62. Zhang FP, Lu QM, Zhang X, Zhang JX (2013) Electrical transport properties of CaMnO3 thermoelectric compound: a theoretical study. J Phys Chem Solids 74:1859–1864
63. Koumoto K et al (2013) Thermoelectric ceramics for energy harvesting. J Am Ceram Soc 96:1–23
64. Srivastava D et al (2015) Crystal structure and thermoelectric properties of Sr-Mo substituted CaMnO3: a combined experimental and computational study. J Mater Chem C 3:12245–12259
65. Bose RSC, Nag A (2016) Effect of dual-doping on the thermoelectric transport properties of CaMn1-xNbx/2Tax/2O3. RSC Adv 6:52318–52325
66. Bhaskar A, Liu CJ, Yuan JJ (2012) Thermoelectric and magnetic properties of Ca0.98RE0.02MnO3-delta (RE = Sm, Gd, and Dy). J Electron Mater 41:2338–2344
67. Taguchi H, Nagao M, Sato T, Shimada M (1989) High-temperature phase-transition of Camno3-Delta. J Solid State Chem 78:312–315. https://doi.org/10.1016/0022-4596(89)90113-8
68. Xu GJ et al (2004) High-temperature transport properties of Nb and Ta substituted CaMnO3 system. Solid State Ionics 171:147–151
69. Bocher L et al (2008) CaMn1-xNbxO3 (x <= 0.08) perovskite-type phases as promising new high-temperature n-type thermoelectric materials. Inorg Chem 47:8077–8085
70. Miclau M et al (2007) Structural and magnetic transitions in CaMn1-xWxO3. Chem Mater 19:4243–4251
71. Thiel P et al (2013) Influence of tungsten substitution and oxygen deficiency on the thermoelectric properties of CaMnO3-delta. J Appl Phys 114:243707
72. Kabir R et al (2015) Role of Bi doping in thermoelectric properties of CaMnO3. J Alloys Compd 628:347–351
73. Park JW, Kwak DH, Yoon SH, Choi SC (2009) Thermoelectric properties of Bi, Nb co-substituted CaMnO3 at high temperature. J Alloys Compd 487:550–555
74. Lan JL et al (2010) High-temperature thermoelectric behaviors of fine-grained Gd-doped CaMnO3 ceramics. J Am Ceram Soc 93: 2121–2124
75. Nag A, D'Sa F, Shubha V (2015) Doping induced high temperature transport properties of Ca1-xGdxMn1-xNbxO3 (0 <= x <= 0.1). Mater Chem Phys 151:119–125
76. Riste T, Samuelsen EJ, Otnes K, Feder J (1971) Critical behaviour of SrTiO3 near 105 degrees phase transition. Solid State Commun 9:1455
77. Mattheiss LF (1972) Energy-bands for KNiF3, SrTiO3, KMoO3, and KTaO3. Phys Rev B 6:4718–4740
78. Ahrens M, Merkle R, Rahmati B, Maier J (2007) Effective masses of electrons in n-type SrTiO3 determined from low-temperature specific heat capacities. Physica B 393:239–248
79. Dehkordi AM et al (2014) Large thermoelectric power factor in Pr-doped SrTiO3-delta ceramics via grain-boundary-induced mobility enhancement. Chem Mater 26:2478–2485
80. Ohta S, Nomura T, Ohta H, Koumoto K (2005) High-temperature carrier transport and thermoelectric properties of heavily La- or Nb-doped SrTiO3 single crystals. J Appl Phys 97:034106
81. Okuda T, Nakanishi K, Miyasaka S, Tokura Y (2001) Large thermoelectric response of metallic perovskites: Sr1-xLaxTiO3 (0 <= x <= 0.1). Phys Rev B 63:113104
82. Walia S et al (2013) Transition metal oxides—thermoelectric properties. Prog Mater Sci 58:1443–1489
83. Ohta H (2007) Thermoelectrics based on strontium titanate. Mater Today 10:44–49
84. Okinaka N, Zhang LH, Akiyama T (2010) Thermoelectric properties of rare earth-doped SrTiO3 using combination of combustion synthesis (CS) and spark plasma sintering (SPS). ISIJ Int 50: 1300–1304
85. Wang HC et al (2011) Doping effect of La and Dy on the thermoelectric properties of SrTiO3. J Am Ceram Soc 94:838–842
86. Vaseem M, Umar A, Hahn Y-B (2010) ZnO nanoparticles: growth, properties and applications In: Metal Oxide Nanostructures and Their Application, vol 5. American Scientific Publishers, New York, pp 1–36
87. Hussain B, Raja MYA, Lu N, Ferguson IT (2013) Application and synthesis of zinc oxide: an emerging wide bandgap material. High Capacity Optical Networks and Enabling Technologies (HONET-CNS), 2013 10th International Conference, IEEE, Cyprus, pp 88–93
88. Jood P, Mehta RJ, Zhang Y, Peleckis G, Wang X, Siegel RW, Borca-Tasciuc T, Dou S, Ramanath G (2011) Al-doped zinc oxide nanocomposites with enhanced thermoelectric properties. Nano Lett 11:4337–4342
89. Ma N, Li JF, Zhang BP, Lin YH, Ren LR, Chen GF (2010) Microstructure and thermoelectric properties of Zn1−xAlxO ceramics fabricated by spark plasma sintering. J Phys Chem Solids 71:1344–1349
90. Hussain B et al (2014) Is ZnO as a univeral semiconductor material an oxymoron? Proc of SPIE. International Society for Optics and Photonics, pp 898718-898718-14

91. Kucukgok B, Wang B, Melton AG, Lu N, Ferguson IT (2014) Comparison of thermoelectric properties of GaN and ZnO samples. Phy Status Solidi C 11:894–897
92. Tsubota T, Ohtaki M, Eguchi K, Arai H (1997) Thermoelectric properties of Al-doped ZnO as a promising oxidematerial for high-temperature thermoelectric conversion. J Mater Chem 7:85–90
93. Ohtaki M, Araki K, Yamamoto K (2009) High thermoelectric performance of dually doped ZnO ceramics. J Electron Mater 38:1234–1238
94. Park K, Hwang H, Seo J, Seo W-S (2013) Enhanced high-temperature thermoelectric properties of Ce-and Dy-doped ZnO for power generation. Energy 54:139–145
95. Chappel S, Zaban A (2002) Nanoporous SnO2 electrodes for dye-sensitized solar cells: improved cell performance by the synthesis of 18nm SnO2 colloids. Sol Energy Mater Sol Cells 71:141–152
96. Olivi P, Pereira EC, Longo E, Varella JA, Bulhoes S (1993) Preparation and characterization of a dip-coated SnO2 film for transparent electrodes for transmissive electrochromic decives. J Electrochem Soc 140:L81_L82
97. Sekizawa K, Widjaja H, Maeda S, Ozawa Y, Eguchi K (2000) Low temperature oxidation of methane over Pd/SnO2 catalyst. Appl Catal A Gen 200:211–217
98. Bueno P et al (1998) Investigation of the electrical properties of SnO2 varistor system using impedance spectroscopy. J Appl Phys 84:3700
99. Leite ER, Weber IT, Longo E, Varela JA (2000) A new method to control particle size and particle size distribution of SnO2 nanoparticles for gas sensor applications. Adv Mater 12:965
100. Rubenis K et al (2017) Thermoelectric properties of dense Sb-doped SnO2 ceramics. J Alloys Compd 692:515–521
101. Yanagiya S, Nong N, Xu GJ, Sonne M, Pryds N (2011) Thermoelectric properties of SnO2 ceramics doped with Sb and Zn. J Electron Mater 40:674–677
102. Tsubota T, Kobayashi S, Murakami N, Ohno T (2014) Improvement of thermoelectric performance for Sb-doped SnO2 ceramics material by addition of Cu as sintering additive. J Electron Mater 43:3567
103. Tsubota T, Ohno T, Shiraishi N, Miyazaki Y (2008) Thermoelectric properties of Sn1-x-yTiySbxO2 ceramics. J Alloys Compd 463:288–293
104. Berardan D, Guilmeau E, Maignan A, Raveau B (2008) In2O3: Ge, a promising n-type thermoelectric oxide composite. Solid State Commun 146:97–101
105. van Hest MFAM, Dabney MS, Perkins JD, Ginley DS (2006) High-mobility molybdenum doped indium oxide. Thin Solid Films 496:70–74
106. Meng Y et al (2001) A new transparent conductive thin film In2O3: Mo. Thin Solid Films 394:219–223
107. van Hest MFAM, Dabney MS, Perkins JD, Ginley DS, Taylor MP (2005) Titanium-doped indium oxide: a high-mobility transparent conductor. Appl Phys Lett 87:032111
108. Koida T, Kondo M (2007) Comparative studies of transparent conductive Ti-, Zr-, and Sn-doped In2O3 using a combinatorial approach. J Appl Phys 101:063713
109. Li XF, Zhang Q, Miao WN, Huang L, Zhang ZJ (2006) Transparent conductive oxide thin films of tungsten-doped indium oxide. Thin Solid Films 515:2471–2474
110. Liu Y et al (2010) Effect of transition-metal cobalt doping on the thermoelectric performance of In2O3 ceramics. J Am Ceram Soc 93:2938–2941
111. Liu Y et al (2015) Enhanced thermoelectric properties of Ga-doped In2O3 ceramics via synergistic band gap engineering and phonon suppression. Phys Chem Chem Phys 17:11229–11233
112. Matsubara I et al (2001) Fabrication of an all-oxide thermoelectric power generator. Appl Phys Lett 78:3627
113. Man EA, Schaltz E, Rosendahl L, Rezaniakolaei A, Platzek D (2015) A high temperature experimental characterization procedure for oxide-based thermoelectric generator modules under transient conditions. Energies 8:12839–12847
114. Zhou CL et al (2017) ZnO for solar cell and thermoelectric applications. Proc SPIE 10105:101051K–1101051
115. Wang N et al (2013) Enhanced thermoelectric performance of Nb-doped SrTiO3 by nano-inclusion with low thermal conductivity. Sci Rep 3:3449
116. Xu T et al (2017) Superior Cu2S/brass-mesh electrode in CdS quantum dot sensitized solar cells for dual-side illumination. Mater Lett 195:100–103
117. Liu T et al (2017) Ni nanobelts induced enhancement of hole transport and collection for high efficiency and ambient stable mesoscopic perovskite solar cells. J Mater Chem A 5:4292–4299
118. Hu W et al (2017) Hematite electron-transporting layers for environmentally stable planar perovskite solar cells with enhanced energy conversion and lower hysteresis. J Mater Chem A 5:1434–1441
119. Rajan J, Thavasi V, Ramakrishna S (2009) Metal oxides for dye-sensitized solar cells. J Am Ceram Soc 92:13
120. Durr M, Rosselli S, Yasuda A, Nelles G (2006) Band-gap engineering of metal oxides for dye-sensitized solar cells. J Phys Chem B 110:4
121. Barbi GB, Santos JP, Serrini P, Gibson PN, Horrillo MC, Manes L (1995) Ultrafine grain-size tin-oxide films for carbon monoxide monitoring in urban environments. Sensors Actuators: B Chem 25:5

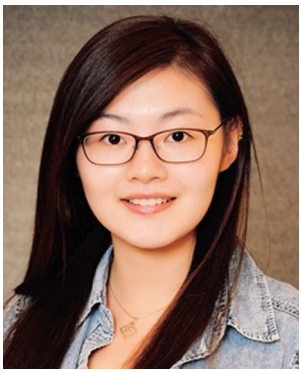

Yining Feng is pursuing her PhD degree of Civil Engineering at Purdue University. She is also a guest graduate student at Argonne National Lab. Her current research interests range from nanostructured oxides for high temperature thermoelectric applications to flexible thermoelectric devices for medium to low temperature applications. Yining has published one book chapter, four journal papers and one conference proceeding. Yining has attended the 2017 National Science Foundation (NSF) Innovation Corps (I-Corps) as an entrepreneur lead on high temperature thermoelectric technology development.

Ian Ferguson currently based at Missouri University of Science and Technology (Missouri S&T), most recently, as the founding Vice Provost and Dean of the College of Engineering Computing. His research has focused on building interdisciplinary teams to use compound semiconductor materials and devices for applications in the areas of sensors, illumination, energy harvesting, and spintronics. He has active research collaborations in the US, Europe, and Asia, which has resulted in over 490 refereed journals and conference papers. He has been actively involved in the entrepreneurial process of establishing new companies has co-founded a business incubator, PiES, that was named

one of the "5 Incubators That Are Shaping the Future of Green Business". He is a Fellow of the Royal Society of Arts, Manufactures and Commerce (FRSA) and Fellow of IEEE, IOP and SPIE.

Na (Luna) Lu is an associate professor of the Lyles School of Civil Engineering, School of Materials Engineering (by Courtesy) and Birck Nanotechnology Center at Purdue University. She is leading a multi-disciplinary research group that develops nanostructured materials and devices for energy harvesting, sensing and non-destructive testing. Lu has authored over 60 referred publications; one book, four book chapters, one patent and three provisional patents. She has given numerous keynote and invited talks at top research conferences, including Material Research Society (MRS), The Mineral, Metals and Materials (TMS), and SPIE Photonic West, etc. Lu has won several scientific awards, including the 2014 National Science Foundation (NSF) CAREER Award. She has also founded a spin-off company with the technologies invented at her research lab.